



# TOI-3235 b: A Transiting Giant Planet around an M4 Dwarf Star

Melissa J. Hobson<sup>1,2</sup> , Andrés Jordán<sup>2,3,4</sup> , E. M. Bryant<sup>5,6,7</sup> , R. Brahm<sup>2,3,4</sup> , D. Bayliss<sup>5</sup> , J. D. Hartman<sup>8</sup> , G. Á. Bakos<sup>8</sup> , Th. Henning<sup>1</sup> , Jose Manuel Almenara<sup>9</sup> , Khalid Barkaoui<sup>10,11,12</sup> , Zouhair Benkhaldoun<sup>13</sup> , Xavier Bonfils<sup>9</sup> , François Bouchy<sup>14</sup> , David Charbonneau<sup>15</sup> , Marion Cointepas<sup>9,14</sup> , Karen A. Collins<sup>15</sup> , Jason D. Eastman<sup>15</sup> , Mourad Ghachoui<sup>10,13</sup> , Michaël Gillon<sup>10</sup> , Robert F. Goetze<sup>16</sup> , Keith Horne<sup>17</sup> , Jonathan M. Irwin<sup>18</sup> , Emmanuel Jehin<sup>19</sup> , Jon M. Jenkins<sup>20</sup> , David W. Latham<sup>15</sup> , Dan Moldovan<sup>21</sup> , Felipe Murgas<sup>9,22,23</sup> , Francisco J. Pozuelos<sup>10,19,24</sup> , George R. Ricker<sup>16</sup> , Richard P. Schwarz<sup>15</sup> , S. Seager<sup>16,25,26</sup> , Gregor Srdoc<sup>27</sup> , Stephanie Striegel<sup>28</sup> , Mathilde Timmermans<sup>10</sup> , Andrew Vanderburg<sup>16</sup> , Roland Vanderspek<sup>16</sup> , and Joshua N. Winn<sup>29</sup>

<sup>1</sup> Max Planck Institute for Astronomy, Königstuhl 17, D-69117—Heidelberg, Germany; [hobson@mpia.de](mailto:hobson@mpia.de)

<sup>2</sup> Millennium Institute of Astrophysics (MAS), Nuncio Monseñor Sótero Sanz 100, Providencia, Santiago, Chile

<sup>3</sup> Facultad de Ingeniería y Ciencias, Universidad Adolfo Ibáñez, Av. Diagonal las Torres 2640, Peñalolén, Santiago, Chile

<sup>4</sup> Data Observatory Foundation, Santiago, Chile

<sup>5</sup> Department of Physics, University of Warwick, Gibbet Hill Road, Coventry CV4 7AL, UK

<sup>6</sup> Centre for Exoplanets and Habitability, University of Warwick, Gibbet Hill Road, Coventry CV4 7AL, UK

<sup>7</sup> Mullard Space Science Laboratory, University College London, Holmbury St Mary, Dorking, Surrey, RH5 6NT, UK

<sup>8</sup> Department of Astrophysical Sciences, Princeton University, NJ 08544, USA

<sup>9</sup> Univ. Grenoble Alpes, CNRS, IPAG, F-38000 Grenoble, France

<sup>10</sup> Astrobiology Research Unit, Université de Liège, 19C Allée du 6 Août, B-4000 Liège, Belgium

<sup>11</sup> Department of Earth, Atmospheric and Planetary Science, Massachusetts Institute of Technology, 77 Massachusetts Avenue, Cambridge, MA 02139, USA

<sup>12</sup> Instituto de Astrofísica de Canarias (IAC), Calle Vía Láctea s/n, E-38200, La Laguna, Tenerife, Spain

<sup>13</sup> Oukaimeden Observatory, High Energy Physics and Astrophysics Laboratory, Faculty of Sciences Semlalia, Cadi Ayyad University, Marrakech, Morocco

<sup>14</sup> Observatoire de Genève, Département d'Astronomie, Université de Genève, Chemin Pegasi 51b, 1290 Versoix, Switzerland

<sup>15</sup> Center for Astrophysics | Harvard & Smithsonian, 60 Garden Street, Cambridge, MA 02138, USA

<sup>16</sup> Department of Physics and Kavli Institute for Astrophysics and Space Research, Massachusetts Institute of Technology, Cambridge, MA 02139, USA

<sup>17</sup> SUPA Physics and Astronomy, University of St. Andrews, Fife, KY16 9SS Scotland, UK

<sup>18</sup> Institute of Astronomy, University of Cambridge, Madingley Road, Cambridge, CB3 0HA, UK

<sup>19</sup> Space sciences, Technologies and Astrophysics Research (STAR) Institute, Université de Liège, Belgium

<sup>20</sup> NASA Ames Research Center, Moffett Field, CA 94035, USA

<sup>21</sup> Google, Cambridge, MA, USA

<sup>22</sup> Instituto de Astrofísica de Canarias (IAC), E-38200 La Laguna, Tenerife, Spain

<sup>23</sup> Dept. Astrofísica, Universidad de La Laguna (ULL), E-38206 La Laguna, Tenerife, Spain

<sup>24</sup> Instituto de Astrofísica de Andalucía (IAA-CSIC), Glorieta de la Astronomía s/n, E-18008 Granada, Spain

<sup>25</sup> Department of Earth, Atmospheric and Planetary Sciences, Massachusetts Institute of Technology, Cambridge, MA 02139, USA

<sup>26</sup> Department of Aeronautics and Astronautics, MIT, 77 Massachusetts Avenue, Cambridge, MA 02139, USA

<sup>27</sup> Kotizarovci Observatory, Sarsoni 90, 51216 Viskovo, Croatia

<sup>28</sup> San Jose State University, 1 Washington Square, San Jose, CA 95192, USA

<sup>29</sup> Department of Astrophysical Sciences, Princeton University, 4 Ivy Lane, Princeton, NJ 08544, USA

Received 2022 December 15; revised 2023 February 16; accepted 2023 February 17; published 2023 March 21

## Abstract

We present the discovery of TOI-3235 b, a short-period Jupiter orbiting an M dwarf with a stellar mass close to the critical mass at which stars transition from partially to fully convective. TOI-3235 b was first identified as a candidate from TESS photometry and confirmed with radial velocities from ESPRESSO and ground-based photometry from HATSouth, MEarth-South, TRAPPIST-South, LCOGT, and ExTrA. We find that the planet has a mass of  $0.665 \pm 0.025 M_J$  and a radius of  $1.017 \pm 0.044 R_J$ . It orbits close to its host star, with an orbital period of 2.5926 days but has an equilibrium temperature of  $\approx 604$  K, well below the expected threshold for radius inflation of hot Jupiters. The host star has a mass of  $0.3939 \pm 0.0030 M_\odot$ , a radius of  $0.3697 \pm 0.0018 R_\odot$ , an effective temperature of 3389 K, and a *J*-band magnitude of  $11.706 \pm 0.025$ . Current planet formation models do not predict the existence of gas giants such as TOI-3235 b around such low-mass stars. With a high transmission spectroscopy metric, TOI-3235 b is one of the best-suited giants orbiting M dwarfs for atmospheric characterization.

*Unified Astronomy Thesaurus concepts:* Exoplanets (498); Transit photometry (1709); Radial velocity (1332); M dwarf stars (982)

*Supporting material:* machine-readable table

## 1. Introduction

While planets around M dwarf stars are extremely abundant (e.g., Dressing & Charbonneau 2015; Hirano et al. 2018;

Mulders 2018; Hsu et al. 2020), the vast majority of these planets are smaller than Neptune, particularly around less massive M dwarfs ( $M < 0.5 M_\odot$ ). Standard core-accretion formation models have long predicted few Jovian-mass planets around these less massive M dwarfs (e.g., Laughlin et al. 2004, who also anticipate a particular scarcity of short-period giant planets). More recent implementations such as the Bern model (Burn et al. 2021) reproduce the low-mass planet population very well but predict

Original content from this work may be used under the terms of the [Creative Commons Attribution 4.0 licence](https://creativecommons.org/licenses/by/4.0/). Any further distribution of this work must maintain attribution to the author(s) and the title of the work, journal citation and DOI.

few gas giants around all M dwarfs, and cannot produce them around later M dwarfs with  $M < 0.5M_{\odot}$  without fine-tuning of the planetary migration (Schlecker et al. 2022). Even prior to the Transiting Exoplanet Survey Satellite (TESS; Ricker et al. 2015) mission, there were discoveries that challenged this (such as Kepler-45 b, Johnson et al. 2012; HATS-6 b, Hartman et al. 2015; NGTS-1 b, Bayliss et al. 2018). More recently, both TESS and radial velocity (RV) surveys have added to the known giant planets orbiting low-mass stars (e.g., GJ 3512 b, Morales et al. 2019; TOI-3884 b, Almenara et al. 2022), suggesting a potential alternative formation pathway such as gravitational instability (e.g., Boss 2006). However, as noted by Schlecker et al. (2022), gravitational instability is expected to form very massive planets of  $\approx 10M_J$  on large orbits, while the planets found to date are mainly of Jupiter mass, and many have short orbital periods. Likewise, most of these planets orbit early M dwarfs, for which the Bern model can, though rarely, produce gas giants; the first, and until now only, exception was TOI-5205 b (Kanodia et al. 2023), which orbits an M4 star. It is also worth noting that the Bern models normally assume a smooth initial gas surface density distribution in the protoplanetary disk; a nonsmooth density distribution could modify the migration history and potentially facilitate the formation of these planets.

In this context, the discovery and characterization of giant planets around M dwarfs, particularly later M dwarfs, are of paramount importance to planetary formation and migration theory. Transiting planets confirmed by RVs, for which both the mass and radius can be measured, are especially valuable. In this Letter, we present the transiting gas giant TOI-3235 b, orbiting an M4 star with a period of 2.5926 days. It is only the second gas giant found to orbit a later M dwarf on the boundary between partially and fully convective M dwarfs (Chabrier & Baraffe 1997) and is one of a mere dozen giant planets orbiting M dwarf stars. The planet was first identified as a candidate by the TESS mission and confirmed with ground-based photometry from HATSouth, MEarth-South, TRAPPIST-South, Las Cumbres Observatory global telescope network (LCOGT), and Exoplanets in Transits and their Atmospheres (ExTrA), and RVs from the Echelle SPectrograph for Rocky Exoplanets and Stable Spectroscopic Observations (ESPRESSO).

We present the data in Section 2. The analysis is described in Section 3. Finally, we discuss and summarize our findings in Section 4.

## 2. Observations

### 2.1. Photometry

#### 2.1.1. TESS

TOI-3235 was observed by the TESS primary and extended missions, in sectors 11 (2019 April 23rd to May 20th) and 38 (2021 April 29th to May 26th), respectively. In both cases, it was observed with camera 2 and CCD 4. The long-cadence data (30 minute cadence for sector 11; 10 minute cadence for sector 38) were initially processed by the Quick-Look Pipeline (QLP; Huang et al. 2020a, 2020b), which uses full-frame images calibrated by the *tica* package (Fausnaugh et al. 2020). The TESS faint-star search (Kunimoto et al. 2022) detected a planet in the QLP data, and it was promoted to a TOI following Guerrero et al. (2021), as noted in the ExoFOP archive.<sup>30</sup> For our analysis, we downloaded the TESS

PDCSAP light curves (Smith et al. 2012; Stumpe et al. 2012, 2014) processed by the TESS Science Processing Operation Center (SPOC; Jenkins et al. 2016) pipeline at NASA Ames Research Center, from the TESS-SPOC High Level Science Product on MAST (Caldwell et al. 2020). The SPOC difference image centroiding analysis locates the source of the transit signal to within  $3''.3 \pm 2''.5$  of the target star (Twicken et al. 2018). The TESS light curves are shown in Figure 1, and the data listed in Table 1.

#### 2.1.2. HATSouth

HATSouth (Bakos et al. 2013) is a network of 24 telescopes, distributed in three sites at Las Campanas Observatory (LCO) in Chile, the site of the H.E.S.S. gamma-ray observatory in Namibia, and Siding Spring Observatory in Australia. Each telescope has a 0.18 m aperture and  $4K \times 4K$  front-illuminated CCD cameras. HATSouth observed TOI-3235 from 2017 February 11th through 2017 May 15th from all three sites. The data were reduced as described in Penev et al. (2013). The transit was clearly detected but was not flagged by the automated search due to the high transit depth and the pre-Gaia poor constraint on the stellar size from *J-K* magnitudes. The light curve is shown in Figure 2 (left panel), and the data are listed in Table 1.

#### 2.1.3. MEarth-South

MEarth-South is an array of eight 0.4 m telescopes at the Cerro Tololo Inter-American Observatory (CTIO) in Chile (Nutzman & Charbonneau 2008; Irwin et al. 2015). MEarth observed TOI-3235 with six telescopes on 2021 June 21st in the RG715 filter with 60 s exposure time, obtaining a full transit of TOI-3235.01. The light curves are shown in Figure 2 (right panel), where the data from all six telescopes have been plotted together, and the data are listed in Table 1.

#### 2.1.4. TRAPPIST-South

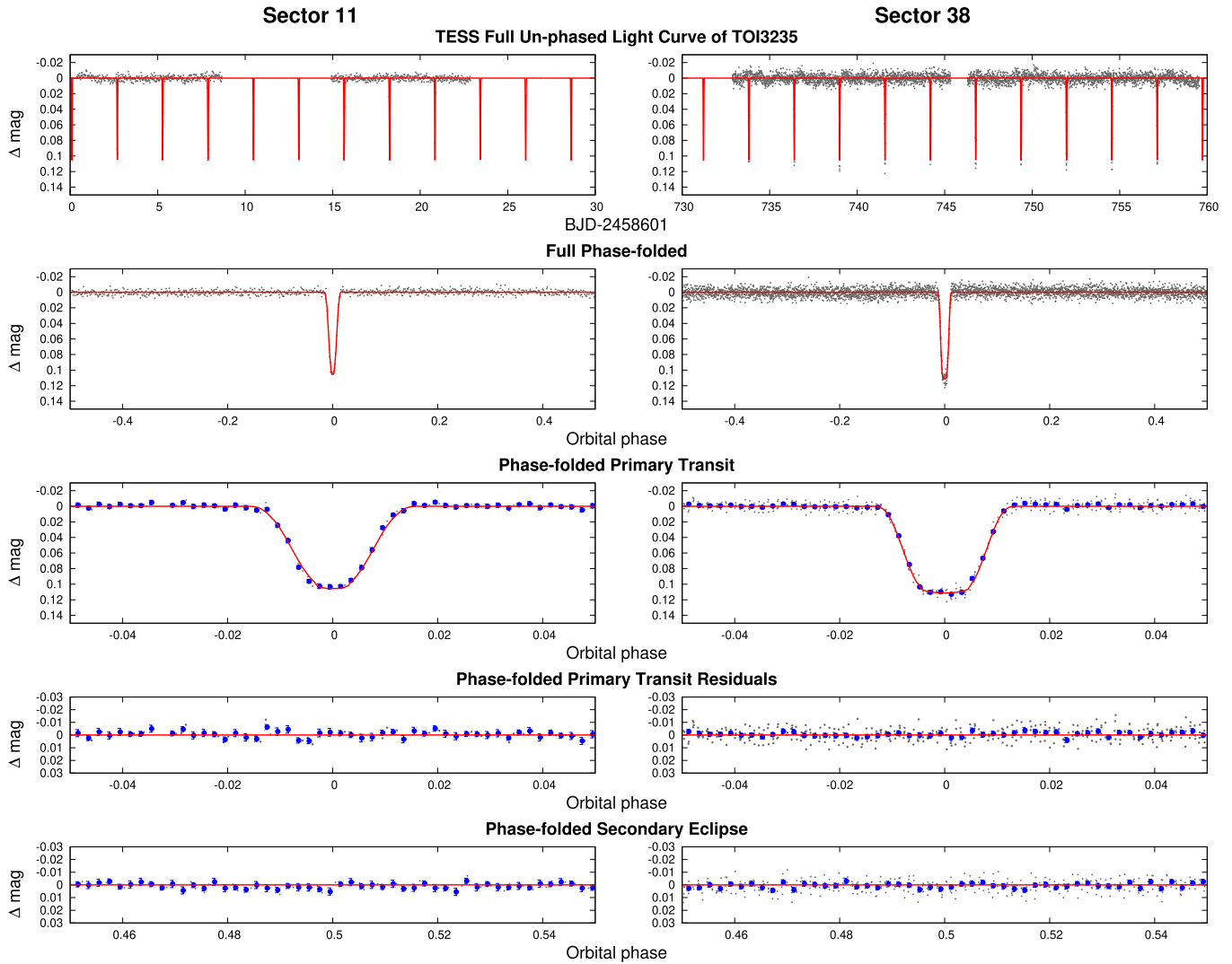
TRAPPIST-South (Gillon et al. 2011; Jehin et al. 2011) is a 0.6 m Ritchey–Chrétien robotic telescope at La Silla Observatory in Chile, equipped with a  $2K \times 2K$  back-illuminated CCD camera with a pixel scale of  $0''.65 \text{ pixel}^{-1}$ , resulting in a field of view of  $22' \times 22'$ . A full transit of TOI-3235.01 was observed by TRAPPIST-South on 2022 May 10th in the Sloan-*z'* filter with an exposure time of 100 s. We used the TESS Transit Finder tool, which is a customized version of the Tapir software package (Jensen 2013), to schedule the observations. Data reduction and photometric measurement were performed using the PROSE<sup>31</sup> pipeline (Garcia et al. 2022). The light curve is shown in Figure 2 (right panel), and the data are listed in Table 1.

#### 2.1.5. LCOGT

The LCOGT network (Brown et al. 2013) is a globally distributed network of 1 m telescopes. The telescopes are equipped with  $4096 \times 4096$  SINISTRO cameras having an image scale of  $0''.389$  per pixel, resulting in a  $26' \times 26'$  field of view. TOI-3235 was observed by LCOGT with the SINISTRO instrument at the South Africa Astronomical Observatory site in the Sloan-*i'* band on 2021 June 10th and

<sup>30</sup> Located at <https://exofop.ipac.caltech.edu/tess/target.php?id=243641947>.

<sup>31</sup> PROSE: <https://github.com/lgrcia/prose>.



**Figure 1.** TESS long-cadence light curves for TOI-3235 for sector 11 (left column; 30 minute cadence) and sector 38 (right column; 10 minute cadence). For each sector, we show the full unphased light curve as a function of time (top row); the full phase-folded light curve (second row); the phase-folded light curve zoomed in on the planetary transit (third row); the residuals from the best-fit model, the phase-folded residuals from the best-fit model, zoomed in on the planetary transit (fourth row); and the phase-folded light curve zoomed in on the secondary eclipse (bottom row). The solid red line in each panel shows the model fit to the light curve. The blue filled circles show the light curve binned in phase with a bin size of 0.002. Other observations included in our analysis of this system are shown in Figures 2 and 3.

at the CTIO site in the Sloan- $g'$  band on 2022 July 1st, full transits of TOI-3235.01 being obtained in both observations. We used the TESS Transit Finder, which is a customized version of the Tapir software package (Jensen 2013), to schedule our transit observations. The images were calibrated by the standard LCOGT BANZAI pipeline (McCully et al. 2018). The differential photometric data were extracted using AstroImageJ (Collins et al. 2017). The light curves are shown in Figure 2 (right panel), and the data listed in Table 1.

### 2.1.6. ExTrA

The ExTrA facility (Shaklan et al. 2015) is composed of a near-infrared (0.85–1.55  $\mu\text{m}$ ) multiobject spectrograph fed by three 0.6 m telescopes located at La Silla observatory in Chile. We observed five full transits of TOI-3235.01 on 2022 March 2nd (with three telescopes) and on 2022 March 28th, 2022 April 2nd, 2022 April 23rd, and 2022 May 24th (with two telescopes). We observed using the fibers with 8'' apertures and used the low-resolution mode of the spectrograph ( $R \sim 20$ ) and 60 s exposures for all nights. At the focal plane of each telescope, five fiber

positioners are used to pick the light from the target and four comparison stars. As comparison stars, we observed 2MASS J13493913-4615443, 2MASS J13515346-4623273, 2MASS J13510825-4612537, and 2MASS J13481046-4615434, with  $J$  magnitude (Skrutskie et al. 2006) and  $T_{\text{eff}}$  (Gaia Collaboration et al. 2018) similar to TOI-3235. The resulting ExTrA data were analyzed using custom data reduction software. The light curves are shown in Figure 2 (right panel), and the data listed in Table 1.

## 2.2. Radial Velocities

### 2.2.1. ESPRESSO

ESPRESSO (Pepe et al. 2021) is an ultrastable fiber-fed échelle high-resolution spectrograph installed at the incoherent combined Coude facility of the Very Large Telescope (VLT) in Paranal Observatory, Chile. We observed TOI-3235 with ESPRESSO in high-resolution mode (1 UT,  $R \sim 140,000$ ) between 2022 February 2nd and 14th, obtaining seven spectra under program ID 108.22B4.001 aka 0108.C-0123(A). The

**Table 1**  
Light-curve Data for TOI-3235

BJD <sup>a</sup> (2,450,000+)	Mag <sup>b</sup>	$\sigma_{\text{Mag}}$	Mag(orig) <sup>c</sup>	Filter	Instrument
7,853.13313	13.60729	0.03233	-0.02073	<i>r</i>	HATSouth/G701.3
7,879.05934	13.62317	0.02532	-0.00485	<i>r</i>	HATSouth/G701.3
7,801.28120	13.57721	0.03175	-0.05081	<i>r</i>	HATSouth/G701.3
7,853.13745	13.66479	0.03355	0.03677	<i>r</i>	HATSouth/G701.3
7,879.06378	13.65081	0.02521	0.02279	<i>r</i>	HATSouth/G701.3
7,801.28524	13.61521	0.03411	-0.01281	<i>r</i>	HATSouth/G701.3
7,801.29055	13.67750	0.05744	0.04948	<i>r</i>	HATSouth/G701.3
7,853.14366	13.58338	0.03234	-0.04464	<i>r</i>	HATSouth/G701.3
7,879.06997	13.59425	0.02449	-0.03377	<i>r</i>	HATSouth/G701.3
7,853.14794	13.67704	0.03710	0.04902	<i>r</i>	HATSouth/G701.3

**Notes.** This table is available in a machine-readable form. A portion is shown here for guidance regarding its form and content.

<sup>a</sup> Barycentric Julian Date computed on the Barycentric Dynamical Time (TDB) system with correction for leap seconds.

<sup>b</sup> The out-of-transit level has been subtracted. For observations made with the HATSouth instruments these magnitudes have been corrected for trends using the external parameter decorrelation and trend filtering algorithm procedures applied *prior* to fitting the transit model. This procedure may lead to an artificial dilution in the transit depths when used in its plain mode instead of the signal reconstruction mode (Kovács et al. 2005). The blend factors for the HATSouth light curves are listed in Table 5. For observations made with follow-up instruments (anything other than “HATSouth” in the “Instrument” column), the magnitudes have been corrected for a quadratic trend in time, and for variations correlated with up to three PSF shape parameters, all of which were fitted simultaneously with the transit.

<sup>c</sup> Raw magnitude values without correction for the quadratic trend in time or for trends correlated with the seeing.

(This table is available in its entirety in machine-readable form.)

spectra were reduced with the official ESPRESSO DRS v2.3.5 pipeline (Sosnowska et al. 2015; Modigliani et al. 2020), in the EsoReflex environment (Freudling et al. 2013). The RVs and bisector spans are listed in Table 2, and the phase-folded RVs and bisector spans are shown in Figure 3 (top left and bottom left panels, respectively). Two of the bisector spans are extreme outliers with values of  $< -3000 \text{ m s}^{-1}$ , and were excluded from the analysis.

### 3. Analysis

We carried out a joint analysis of the photometric, astrometric, and RV data for TOI-3235 b following the methods of Hartman et al. (2019) and Bakos et al. (2020). We fit the light-curve data shown in Figures 1 and 2 together with the broadband catalog photometry and Gaia parallax measurement listed in Table 3 and the RV data shown in Figure 3. The model also makes use of the predicted absolute magnitudes in each bandpass from the MIST isochrones and of the extinction, constrained from the SED. We use a Mandel & Agol (2002) transit model with quadratic limb darkening to fit the light curves and assume a Keplerian orbit for fitting the RV measurements. The limb-darkening coefficients are allowed to vary, with priors based on the Claret et al. (2012, 2013) and Claret (2018) theoretical models. The stellar parameters are constrained using isochrones from version 1.2 of the MIST theoretical stellar evolution models (Paxton et al. 2011, 2013, 2015; Choi et al. 2016; Dotter 2016). We allow the line-of-sight extinction  $A_V$  to vary in the fit, imposing a maximum of 0.527 mag and a Gaussian prior of  $0.055 \pm 0.2$  mag based on the MWDUST 3D Galactic extinction model (Bovy et al. 2016).

We used the ODUSSEAS software (Antoniadis-Karnavas et al. 2020), developed specifically for M dwarfs, to measure the  $[\text{Fe}/\text{H}]$  and  $T_{\text{eff}\star}$  from the ESPRESSO spectra. Although ODUSSEAS was developed for spectra with resolutions from 48,000 to 115,000, it has been successfully used with ESPRESSO spectra at their original 140,000 resolution (Lillo-Box et al. 2020). We obtained preliminary values of  $[\text{Fe}/\text{H}] = -0.0024 \pm 0.104$ ,  $T_{\text{eff}\star} = 3196 \pm 67$  K, which were

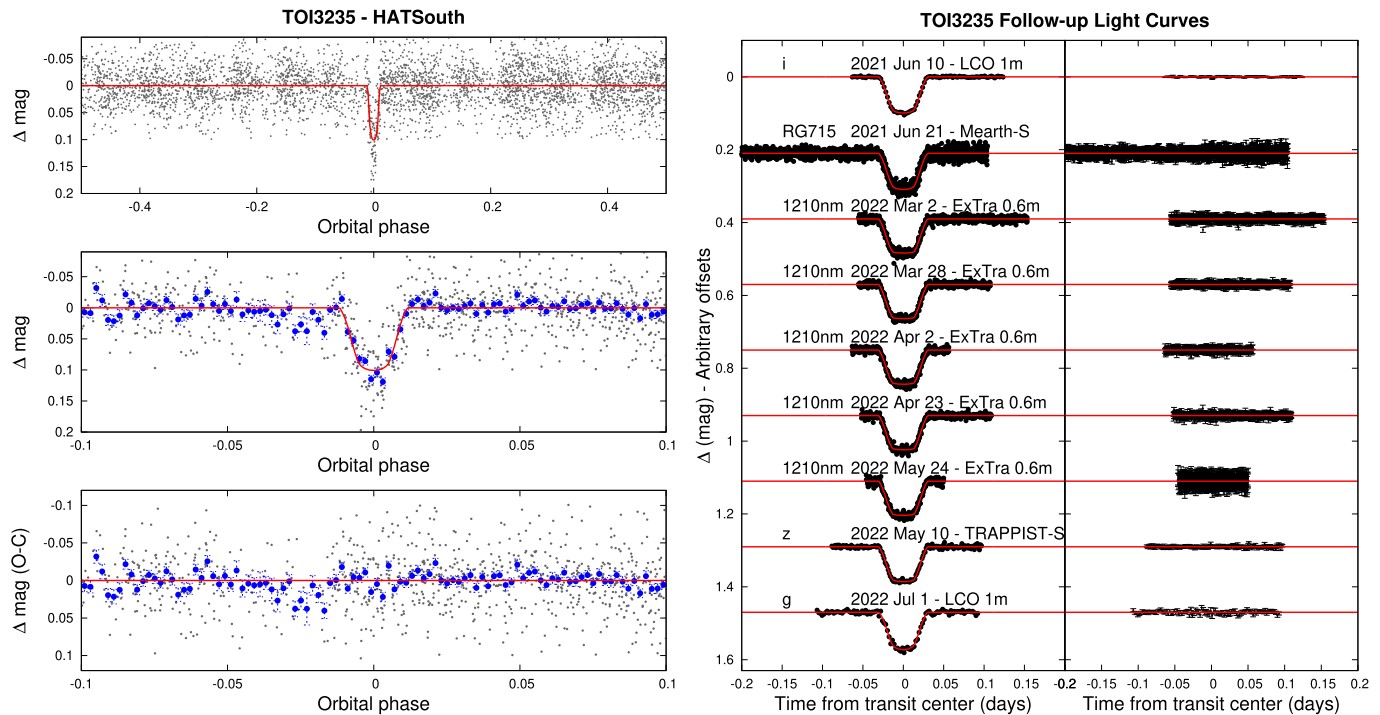
used as priors for the joint analysis,<sup>32</sup> in which a combination of the MIST evolution models, the transit-derived stellar bulk density, and the broadband catalog photometry and parallax are employed to precisely constrain the host star parameters. To determine the spectral type, we used the PyHammer tool (Roulston et al. 2020) with the ESPRESSO spectra, which returned an M5 spectral type. However, color index comparisons with the tables of Pecaut & Mamajek (2013) suggest an earlier spectral type of M3-M4, and visual inspection with the “eyecheck” facility of PyHammer shows an M4 template is also a good match to the spectrum. Therefore, we adopt an M4 spectral type.

We modeled the observations both assuming a circular orbit for the planet, and allowing the orbit to have a nonzero eccentricity. We find that the free-eccentricity model produces an eccentricity consistent with zero ( $e < 0.029$  at 95% confidence). A very low eccentricity is expected, given that we estimate a rapid tidal circularization timescale for this system of  $\sim 6$  Myr (Hut 1981). We therefore adopt the parameters that result from assuming a circular orbit. Applying the transit least squares (TLS; Hippke & Heller 2019) algorithm to the HATSouth and TESS light-curve residuals to the best-fit model finds no additional transit signals. The stellar parameters derived from the analysis assuming a circular orbit are listed in Table 4, while the planetary parameters are listed in Table 5. The best-fit model is shown in Figures 1, 2, and 3. We note that the light-curve uncertainties are scaled up in the fitting procedure to achieve a reduced  $\chi^2$  of unity, but the uncertainties shown in Figure 2 have not been scaled.

The resulting  $\sim 1\%$  and  $\sim 0.5\%$  respective uncertainties on the derived stellar mass and radius are well below the respective  $\sim 5\%$  and  $\sim 4.2\%$  estimated systematic uncertainties of Tayar et al. (2022) for these parameters, which stem from inaccuracies in the fundamental observables and stellar

<sup>32</sup> An independent estimate of  $T_{\text{eff}\star} = 3421 \pm 53$  K can be obtained using the absolute  $G$  magnitude  $M_G$  from Equation (11) of Rabus et al. (2019), which is consistent at  $\approx 2\sigma$  with the value inferred from ODUSSEAS.





**Figure 2.** Ground-based photometry for the the transiting planet system TOI-3235. Left: phase-folded unbinned full HATSouth light curve (top), light curve zoomed in on the transit (middle), and residuals from the best-fit model zoomed in on the transit (bottom). Solid red lines show the best-fit model. Blue circles show the light curves binned in phase with a bin size of 0.002. Right: unbinned follow-up transit light curves corrected for instrumental trends fitted simultaneously with the transit model, which is overplotted (left column), and the residuals to the transit model (right column). Dates, filters, and instruments are indicated. For ExTra we indicate the midpoint of the spectral range. The error bars represent the photon and background shot noise, plus the readout noise.

**Table 2**

Relative Radial Velocities and Bisector Spans from ESPRESSO for TOI-3235

BJD (2,450,000+)	RV <sup>a</sup> (m s <sup>-1</sup> )	$\sigma_{RV}$ <sup>b</sup> (m s <sup>-1</sup> )	BS (m s <sup>-1</sup> )	$\sigma_{BS}$ (m s <sup>-1</sup> )	Phase
9,612.80279	-185.54	4.18	...	...	0.224
9,613.81343	126.16	3.91	...	...	0.613
9,615.71703	-137.66	5.29	38.0	10.6	0.348
9,617.71593	-121.86	4.26	32.6	8.5	0.119
9,618.70340	0.95	5.52	-27.3	11.1	0.499
9,619.86092	53.75	3.50	-12.7	7.0	0.946
9,624.86523	129.76	4.23	-13.9	8.4	0.876

**Notes.**

<sup>a</sup> The zero-point of these velocities is arbitrary. An overall offset  $\gamma$  fitted to the velocities has been subtracted.

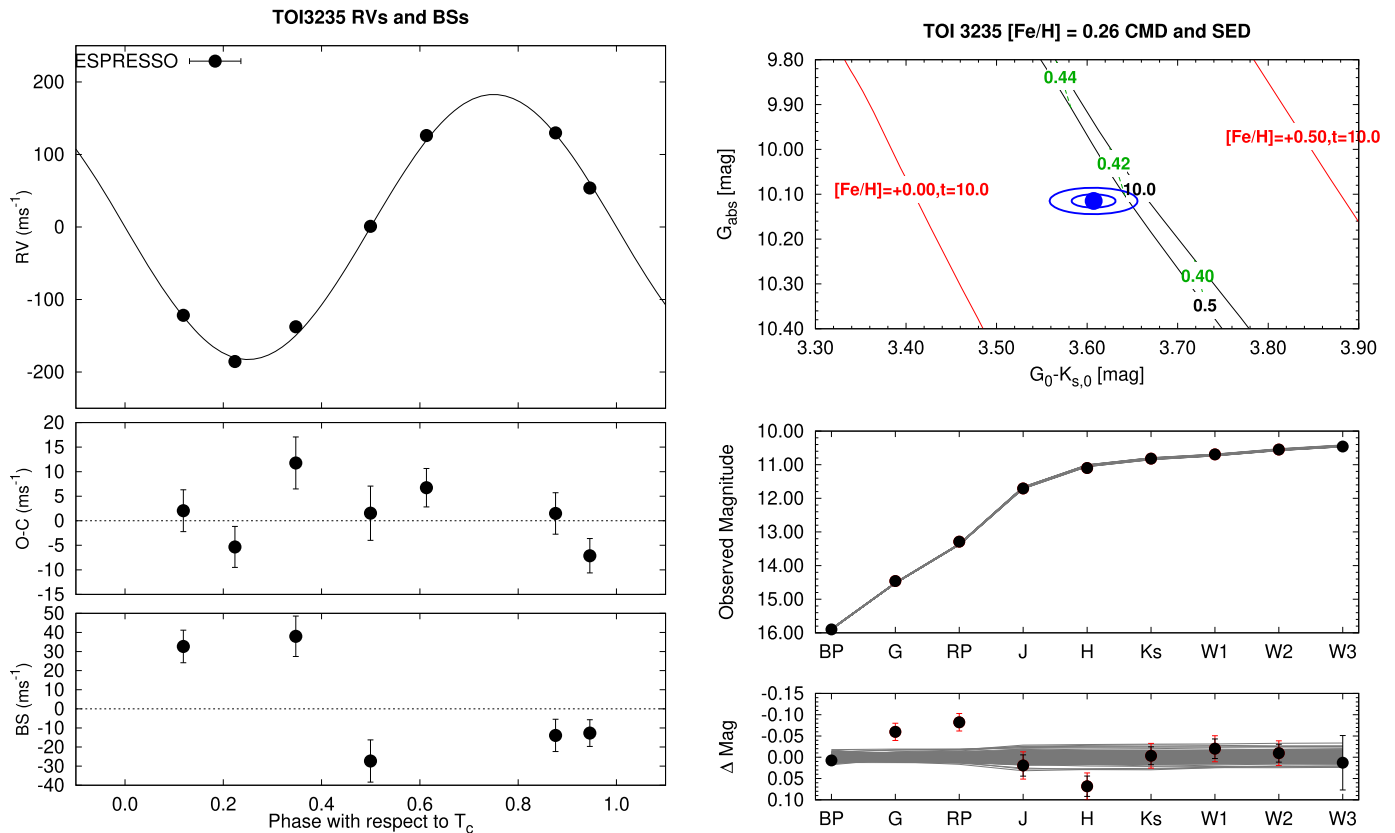
<sup>b</sup> Internal errors excluding the component of astrophysical jitter considered in Section 3.

evolution models. Likewise, the formal uncertainties of 7.4 K on the posterior stellar effective temperature and 0.017 dex on the metallicity are likely quite a bit smaller than the systematic uncertainties, which we may expect to be closer to the ODUSSEAS-derived uncertainties of  $\sim 70$  K and  $\sim 0.1$  dex, respectively. However, as described in Eastman et al. (2022), uncertainties smaller than the general error floors of Tayar et al. (2022) can be achieved for transiting planets by measuring the stellar density  $\rho_*$  directly from the transit and employing it in the derivation of other stellar parameters. Although our fit self-consistently accounts for the relation between the stellar density, transit parameters,  $M_*$ ,  $L_*$ ,  $R_*$ , and  $T_{\text{eff}}$  throughout the fit, as suggested by Eastman et al. (2022), and imposes a constraint that each link in the chain must match a stellar

evolution model, it does not account for systematic errors in those models when imposing this constraint, and thus the formal uncertainties derived in this analysis are too small. Therefore, we conservatively adopt the error floors of Tayar et al. (2022), which we report in brackets in Table 4; for [Fe/H] we report the ODUSSEAS-derived uncertainty. These systematic uncertainties were formally propagated out to the planetary parameters. Regarding the planetary equilibrium temperature  $T_{\text{eq}}$  in particular, it is calculated under the assumptions of 0 albedo and full and instantaneous redistribution of heat, which are unlikely to hold completely in reality but provide a useful approximation.

The formal fit gives a young age of  $0.394^{+0.152}_{-0.090}$  Gyr for the host star. However, this is primarily driven by the photometry being somewhat blue compared to the model values (see Figure 3, top right), which are known to be uncertain for M dwarfs. We see no other evidence of youth such as flares. Likewise, the Generalised Lomb–Scargle periodogram of the HATSouth photometry shows a significant peak at  $44.4264 \pm 0.0010$  days; taking this as the stellar rotation period, the relations of Engle & Guinan (2018) suggest a much larger age of  $\approx 2.7$  Gyr. We also used the BANYAN  $\Sigma$  tool (Gagné et al. 2018) to check the probability of TOI-3235 belonging to known young stellar associations given its Gaia DR3 (Gaia Collaboration et al. 2022) proper motions and RV, finding it has a 99.9% probability of being a field star.

Independent estimates of the stellar mass and radius can be obtained from the  $K_S$  magnitude using the mass–radius–luminosity relations of Mann et al. (2019) and Rabus et al. (2019). Applying these relations leads to a mass of  $M_* = 0.3605 \pm 0.087 M_\odot$  and a radius of  $R_* = 0.37 \pm 0.07 R_\odot$ . While the radius is fully consistent with that obtained via global



**Figure 3.** Left: high-precision RVs from ESPRESSO/VLT phased with respect to the midtransit time, together with the best-fit model, where the center-of-mass velocity has been subtracted (top); RV  $O - C$  residuals (center); and bisector spans (bottom). Error bars include the estimated jitter, which is a free parameter in the fitting. Top right: absolute  $G$  magnitude vs. the dereddened  $G - K_s$  color from Gaia DR2 and 2MASS (filled blue circle) and  $1\sigma$  and  $2\sigma$  confidence regions, including estimated systematic errors in the photometry (blue lines), compared to theoretical isochrones (black lines; ages listed in gigayears) and stellar evolution tracks (green dashed lines; mass listed in solar masses) from the MIST models interpolated at the best-estimate value for the host metallicity. The red lines show isochrones at higher and lower metallicities than the best-estimate value, labeled with their metallicity and age in gigayears. Bottom right: spectral energy distribution (SED) as measured via broadband photometry through the listed filters (top, “Observed Magnitude”) and  $O - C$  residuals from the best-fit model (bottom, “ $\Delta$  Mag”). We plot the observed magnitudes without correcting for distance or extinction. Overplotted are 200 model SEDs randomly selected from the Markov Chain Monte Carlo (MCMC) posterior distribution produced through the global analysis (gray lines). Black error bars show the catalog errors for the broadband photometry measurements; red error bars add an assumed 0.02 mag systematic uncertainty in quadrature to the catalog errors. These latter uncertainties are used in the fit.

modeling, the mass is lower at  $1.5\sigma$ . We choose to adopt the values from the global modeling since it accounts for all variables simultaneously. We also note that the planetary mass and radius calculated by employing the values obtained through the mass–radius–luminosity relations remain consistent with those computed from the global modeling values; thus, adopting the lower stellar mass from the mass–radius–luminosity relations would only make this giant planet even more unusual.

#### 4. Discussion and Conclusions

TOI-3235 b is a close-in Jupiter with  $M_p = 0.665 \pm 0.025 M_J$ ,  $R_p = 1.017 \pm 0.044 R_J$ , orbiting a  $0.3939 \pm 0.0030 M_\odot$  M dwarf with a period of  $2.59261842 \pm 0.00000041$  days. To place it in the context of the M dwarf planet population, in Figure 4 we plot TOI-3235 b together with all other well-characterized planets from the TEPICAT catalog (Southworth 2011) hosted by stars with  $M_* \leq 0.61 M_\odot$  (limit chosen to include  $M_* \approx 0.6 M_\odot$  stars on K-M boundary). In mass–radius space (Figure 4, top panel), TOI-3235 b joins a small cluster of ten giant planets with  $0.8 R_J \leq R_p \leq 1.2 R_J$  and  $0.3 M_J \leq M_p \leq 1.5 M_J$ . Most of these planets (HATS-6 b, Hartman et al. 2015; HATS-74 b and HATS-75 b, Jordán et al. 2022; Kepler-45 b, Johnson et al. 2012; TOI-530 b, Gan et al. 2022; TOI-3714 b, Canas et al. 2022; WASP-80

b, Triaud et al. 2013) are hosted by early M dwarfs with  $M_* \geq 0.5 M_\odot$ . The sole other exception, aside from TOI-3235 b itself, is TOI-5205 b, a Jupiter-sized planet transiting a  $0.392 M_\odot$  star (Kanodia et al. 2023). Save for TOI-530 b, which has a somewhat longer period of 6.39 days, these planets also cluster together in period–radius space (Figure 4, center panel), forming a group of midrange close-in Jupiters with periods between 1.63 and 3.33 days. Likewise, all their host stars except WASP-80 are metal rich (Figure 4, bottom panel), in contrast to the wide range of metallicities shown by the host stars of the lower-mass planets. In particular, TOI-3235 has a metallicity of 0.26. These higher metallicities are consistent with previous findings (e.g., Johnson & Apps 2009; Rojas-Ayala et al. 2010) that M dwarfs hosting giant planets tend to be metal rich. The stellar mass versus planet mass diagram shown in this last panel also highlights the uniqueness of TOI-3235 b and its near twin TOI-5205 b, which inhabit an otherwise empty region of this parameter space.

Despite their clustering in mass–radius space, this group of giant planets spans a fairly wide range of densities, ranging from the very low-density HATS-6 b ( $\rho \approx 0.4 \text{ g cm}^{-3}$ ) to the Jupiter-analog TOI-5205 b ( $\rho \approx 1.3 \text{ g cm}^{-3}$ ) and the high-density HATS-74 b ( $\rho \approx 1.6 \text{ g cm}^{-3}$ ). TOI-3235 b sits in the center of the range, with  $\rho \approx 0.78 \text{ g cm}^{-3}$ , comparable to the density of Saturn. They are all close to the peak of the

**Table 3**  
Astrometric, Spectroscopic, and Photometric Parameters for TOI-3235

Parameter	Value	Source
Astrometric Prop- erties and Cross- identifications		
2MASS-ID	2MASS 13495398-4603583	
TIC-ID	TIC 243641947	
Gaia DR3-ID	GAIA DR3 6107144260251920000	
R.A. (J2000)	13 <sup>h</sup> 49 <sup>m</sup> 53.9777s	Gaia DR3
decl. (J2000)	-46°03′58.4541″	Gaia DR3
$\mu_{R.A.}$ (mas yr <sup>-1</sup> )	-170.503 ± 0.028	Gaia DR3
$\mu_{decl.}$ (mas yr <sup>-1</sup> )	-64.264 ± 0.023	Gaia DR3
Parallax (mas)	13.781 ± 0.027	Gaia DR3
Radial velocity (km s <sup>-1</sup> )	-14.96 ± 2.72	Gaia DR3
Spectroscopic properties		
$T_{\text{eff}\star}$ (K)	3196 ± 67	ODUSSEAS/ ESPRESSO <sup>a</sup>
[Fe/H]	-0.02 ± 0.10	ODUSSEAS/ ESPRESSO <sup>a</sup>
Spectral type	M4	this work
Photometric properties <sup>b</sup>		
$G$ (mag)	14.4605 ± 0.0028	Gaia DR3
$BP$ (mag)	15.9000 ± 0.0042	Gaia DR3
$RP$ (mag)	13.2881 ± 0.0038	Gaia DR3
$J$ (mag)	11.706 ± 0.025	2MASS
$H$ (mag)	11.099 ± 0.024	2MASS
$K_s$ (mag)	10.819 ± 0.021	2MASS
$W1$ (mag)	10.694 ± 0.023	WISE
$W2$ (mag)	10.548 ± 0.021	WISE
$W3$ (mag)	10.458 ± 0.064	WISE

**Notes.**

<sup>a</sup> The ODUSSEAS-derived  $T_{\text{eff}\star}$  and [Fe/H] are not the final adopted parameters but are used as priors for the global modeling.

<sup>b</sup> The listed uncertainties for the photometry are taken from the catalogs. For the analysis we assume a systematic uncertainty floor of 0.02 mag.

**Table 4**  
Derived Stellar Parameters for TOI-3235

Parameter	Value
$M_\star$ ( $M_\odot$ )	0.3939 ± 0.0030 (±0.020)
$R_\star$ ( $R_\odot$ )	0.3697 ± 0.0018 (±0.016)
$\log g_\star$ (cgs)	4.8976 ± 0.0035 (±0.063)
$\rho_\star$ (g cm <sup>-3</sup> )	10.99 ± 0.13
$L_\star$ ( $L_\odot$ )	0.01623 ± 0.00018 (±0.00039)
$T_{\text{eff}\star}$ (K)	3388.8 ± 5.9 (±68)
[Fe/H] (dex)	0.264 <sup>+0.013</sup> <sub>-0.017</sub> (±0.1)
$A_V$ (mag)	0.064 ± 0.021
Distance (pc)	72.50 ± 0.12

**Note.** The listed parameters are those determined through the joint analysis described in Section 3 assuming a circular orbit for the planet. The first uncertainties listed for each parameter are the statistical uncertainties from the fit, not including systematic errors. Values in brackets report the estimated uncertainty floors due to inaccuracies in the fundamental observables and/or the MIST stellar evolution models, where appropriate. These latter floors were formally propagated to the planetary parameter uncertainties.

**Table 5**  
Adopted Orbital and Planetary Parameters for TOI-3235 b

Parameter	Value
Light-curve Parameters	
$P$ (days)	2.59261842 ± 0.00000041
$T_c$ (BJD_TDB) <sup>a</sup>	2,459,690.001730 ± 0.000045
$T_{14}$ (days) <sup>a</sup>	0.06165 ± 0.00021
$T_{12} = T_{34}$ (days) <sup>a</sup>	0.01765 ± 0.00030
$a/R_\star$	15.75 ± 0.73
$c/R_\star$ <sup>b</sup>	44.41 ± 0.32
$R_p/R_\star$	0.2828 ± 0.0016
$b^2$	0.261 <sup>+0.012</sup> <sub>-0.012</sub>
$b \equiv a \cos i/R_\star$	0.511 <sup>+0.011</sup> <sub>-0.012</sub>
$i$ (deg)	88.140 ± 0.046
Dilution factors <sup>c</sup>	
HAT G701/3	0.982 ± 0.022
HAT G701/4	0.957 ± 0.027
TESS Sector 11	1.084 ± 0.011
TESS Sector 38	1.1248 ± 0.0088
Limb-darkening coefficients <sup>d</sup>	
$c_1, T$	0.24 ± 0.12
$c_2, T$	0.33 ± 0.16
$c_1, g$	0.31 ± 0.12
$c_2, g$	0.35 ± 0.14
$c_1, r$	0.41 ± 0.15
$c_2, r$	0.32 ± 0.16
$c_1, z$	0.140 <sup>+0.106</sup> <sub>-0.081</sub>
$c_2, z$	0.17 ± 0.13
$c_1, RG715$	0.30 ± 0.11
$c_2, RG715$	0.26 <sup>+0.11</sup> <sub>-0.15</sub>
RV parameters	
$K$ (m s <sup>-1</sup> )	182.9 ± 3.3
$e^e$	<0.029
RV jitter ESPRESSO (m s <sup>-1</sup> )	<9.6
Planetary parameters	
$M_p$ ( $M_J$ )	0.665 ± 0.025
$R_p$ ( $R_J$ )	1.017 ± 0.044
$C(M_p, R_p)^f$	0.09
$\rho_p$ (g cm <sup>-3</sup> )	0.78 ± 0.11
$\log g_p$ (cgs)	3.202 ± 0.041
$a$ (AU)	0.02709 ± 0.00046
$T_{\text{eq}}$ (K)	604 ± 19
$\Theta^h$	0.0896 ± 0.0042
$\log_{10}(F)$ (cgs) <sup>i</sup>	7.479 ± 0.018

**Notes.** We adopt a model in which the orbit is assumed to be circular. See the discussion in Section 3.

<sup>a</sup> Times are in Barycentric Julian Date calculated on the (TDB) system.  $T_c$ : reference epoch of midtransit that minimizes the correlation with the orbital period.  $T_{14}$ : total transit duration, time between first to last contact;  $T_{12} = T_{34}$ : ingress/egress time, time between first and second, or third and fourth contact.

<sup>b</sup> Reciprocal of the half duration of the transit used as a jump parameter in our MCMC analysis in place of  $a/R_\star$ . It is related to  $a/R_\star$  by the expression  $c/R_\star = a/R_\star(2\pi(1 + e \sin \omega))/(P\sqrt{1 - b^2}\sqrt{1 - e^2})$  (Bakos et al. 2010).

<sup>c</sup> Scaling factor applied to the model transit fit to the HATSouth and TESS light curves. It accounts for dilution of the transit due to blending from neighboring stars, overfiltering of the light curve, or overcorrection of dilution in the TESS SPOC light curves. These factors are varied in the fit, with independent values adopted for each light curve.

<sup>d</sup> Values for a quadratic law. The limb-darkening parameters were directly varied in the fit, using the tabulations from Claret et al. (2012, 2013) and Claret (2018) to place Gaussian priors on their values, assuming a prior uncertainty of 0.2 for each coefficient.

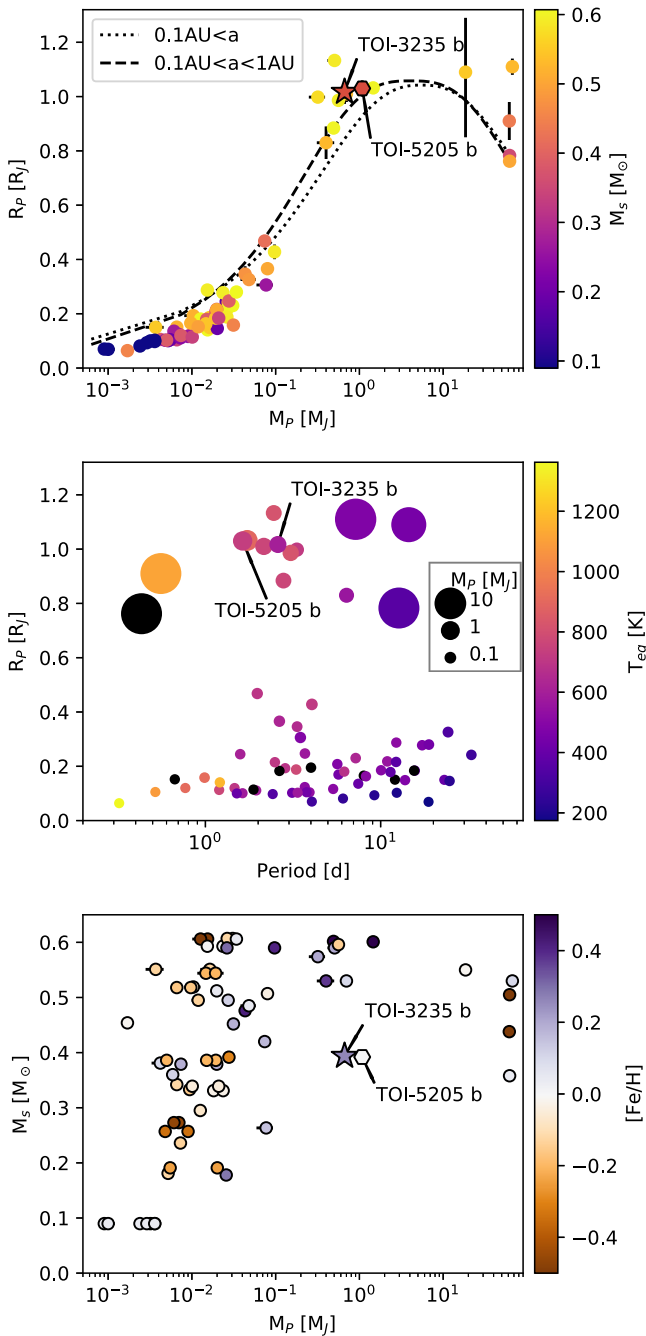
<sup>e</sup> 95% confidence upper limit on the eccentricity determined when  $\sqrt{e} \cos \omega$  and  $\sqrt{e} \sin \omega$  are allowed to vary in the fit.

<sup>f</sup> Term added in quadrature to the formal RV uncertainties for each instrument. It is a free parameter in the fitting routine.

<sup>g</sup> Correlation coefficient between the planetary mass  $M_p$  and radius  $R_p$ , estimated from the posterior parameter distribution.

<sup>h</sup> The Saffronov number is given by  $\Theta = \frac{1}{2}(V_{\text{esc}}/V_{\text{orb}})^2 = (a/R_p)(M_p/M_\star)$  (see Hansen & Barman 2007).

<sup>i</sup> Incoming flux per unit surface area, averaged over the orbit.



**Figure 4.** Top: mass–radius diagram for M dwarf planets with masses and radii measured to better than 25%, as reported in TEPICAT. The markers are color-coded by host star mass. TOI-3235 b and its analog TOI-5205 b are plotted with star and hexagon symbols, respectively, and labeled. Theoretical mass–radius curves from Mordasini et al. (2012) are plotted with dashed and dotted lines. Center: period–radius diagram for the same planets. The markers are scaled by planet mass and color-coded by equilibrium temperature (black when it could not be computed). TOI-3235 b and TOI-5205 b are labeled. Bottom: planet mass vs. stellar mass diagram for the same planets. The markers are color-coded by host star metallicity. TOI-3235 b and TOI-5205 b are plotted with star and hexagon symbols, respectively, and labeled.

theoretical mass–radius relationship derived by Mordasini et al. (2012) (Figure 4, top panel, where we show the relationships for both the full synthetic population and for planets with  $a < 1$  au); save for TOI-530 b, HATS-74 b, and HATS-75 b, which sit on the curve for planets with  $a < 1$  au, and TOI-5205 b, which is consistent with it within error bars, all have larger

radii than predicted. However, although all ten of these giants have periods shorter than the typical 10 d limit taken for hot Jupiters, they have equilibrium temperatures of  $\approx 600$ – $900$  K (Figure 4, center panel), well below the 1000 K limit at which the incident flux is expected to begin to inflate the radii (Demory & Seager 2011; Miller & Fortney 2011; Sarkis et al. 2021). It is also interesting to note that the low-mass planets generally have smaller radii than predicted, suggesting the theoretical relationship—derived from a synthetic population with a fixed stellar mass of  $M_* = 1M_\odot$ —may not be a good fit to M dwarf planets overall.

The similarities between these giant planets may point to similar formation and migration histories. However, the differences in host star mass indicate caution; we may be seeing two distinct populations, one corresponding to early M dwarfs and one corresponding to later M dwarfs. It is thus particularly interesting and relevant to compare TOI-3235 b to TOI-5205 b. Like TOI-5205, TOI-3235 sits on the edge of the Jao Gap, a narrow gap in the Hertzsprung–Russell diagram first identified by Jao et al. (2018) in Gaia data and linked by the authors to the transition between partially and fully convective stars, with  $M_G = 10.04 \pm 0.95$  (Anders et al. 2022), and  $B_P - R_P \approx 2.6$  (Gaia Collaboration et al. 2022). Both these stars are therefore in the transition region between partially and fully convective M dwarfs and as such are likely to undergo periodic changeovers from partially to fully convective and vice versa that alter their radius and luminosity (e.g., van Saders & Pinsonneault 2012; Baraffe & Chabrier 2018). As noted by Silverstein et al. (2022) and Kanodia et al. (2023), these oscillations may impact the planetary orbital parameters and equilibrium temperature. It is possible that the similar planets of these similar stars may share similar formation and/or evolution histories. Kanodia et al. (2023) studied the disk mass necessary to form TOI-5205 b. Since the host stars have the same mass, we can extrapolate from their analysis; the main difference is that TOI-3235 b is rather less massive than TOI-5205 b. As regards planetary heavy-element mass, using the relations of Thorngren et al. (2016) we find a heavy-element mass of  $M_Z \sim 45 M_\oplus$  corresponding to 75% of that of TOI-5205 b; therefore, assuming a solid core and scaling the results of Kanodia et al. (2023), the required disk mass for TOI-3235 b becomes  $\sim 2\%$ – $23\%$  the mass of the host star for 100%–10% formation efficiency, respectively. While lower than the disk mass required to explain TOI-5205 b, given typical disk masses of the order of  $\sim 0.1\%$ – $5\%$  (Pascucci et al. 2016), the formation of TOI-3235 b still requires either an extremely high formation efficiency or a very massive disk.

TOI-3235 b also shows high potential for atmospheric characterization. We compute a transmission spectroscopy metric (TSM; Kempton et al. 2018) of  $\approx 160$ , assuming a scale factor of 1.15. Comparing it to the group of M dwarf planets it clusters with in mass–period–radius space, TOI-3235 b has the second-highest TSM, surpassed only by WASP-80 b (TSM  $\approx 290$ ) and notably higher than its analog TOI-5205 b (TSM  $\approx 100$ ). Atmospheric characterization can help place constraints on the formation and migration history (e.g., Hobbs et al. 2022; Mollière et al. 2022) of this unexpected planet.

We thank the referee for helpful comments that improved this paper.

This paper includes data collected by the TESS mission, which are publicly available from the Mikulski Archive for



Space Telescopes (MAST). The specific observations analyzed can be accessed via [10.17909/mdsd-2297](https://doi.org/10.17909/mdsd-2297). Funding for the TESS mission is provided by NASA’s Science Mission directorate.

This research has made use of the Exoplanet Follow-up Observation Program website, which is operated by the California Institute of Technology, under contract with the National Aeronautics and Space Administration under the Exoplanet Exploration Program.

We acknowledge the use of public TESS data from pipelines at the TESS Science Office and at the TESS Science Processing Operations Center.

Resources supporting this work were provided by the NASA High-End Computing (HEC) Program through the NASA Advanced Supercomputing (NAS) Division at Ames Research Center for the production of the SPOC data products.

Based on observations collected at the European Organisation for Astronomical Research in the Southern Hemisphere under ESO program 0108.C-0123(A).

A.J., R.B., and M.H. acknowledge support from ANID—Millennium Science Initiative—ICN12\_009. A.J. acknowledges additional support from FONDECYT project 1210718. R.B. acknowledges support from FONDECYT Project 1120075 and from project IC120009 “Millennium Institute of Astrophysics (MAS)” of the Millennium Science Initiative. This work was funded by the Data Observatory Foundation.

The MEarth Team gratefully acknowledges funding from the David and Lucile Packard Fellowship for Science and Engineering (awarded to D.C.). This material is based upon work supported by the National Science Foundation under grants AST-0807690, AST-1109468, AST-1004488 (Alan T. Waterman Award), and AST-1616624, and upon work supported by the National Aeronautics and Space Administration under grant No. 80NSSC18K0476 issued through the XRP Program. This work is made possible by a grant from the John Templeton Foundation. The opinions expressed in this publication are those of the authors and do not necessarily reflect the views of the John Templeton Foundation.

The research leading to these results has received funding from the ARC grant for Concerted Research Actions, financed by the Wallonia-Brussels Federation. TRAPPIST is funded by the Belgian Fund for Scientific Research (Fond National de la Recherche Scientifique, FNRS) under the grant PDR T.0120.21. M.G. is F.R.S.-FNRS Research Director and E.J. is F.R.S.-FNRS Senior Research Associate. Observations were carried out from ESO La Silla Observatory.

The postdoctoral fellowship of K.B. is funded by F.R.S.-FNRS grant T.0109.20 and by the Francqui Foundation.

This work makes use of observations from the LCOGT network. Part of the LCOGT telescope time was granted by NOIRLab through the Mid-Scale Innovations Program (MSIP). MSIP is funded by NSF.

Based on data collected under the ExTrA project at the ESO La Silla Paranal Observatory. ExTrA is a project of Institut de Planétologie et d’Astrophysique de Grenoble (IPAG/CNRS/UGA), funded by the European Research Council under the ERC Grant Agreement No. 337591-ExTrA. This work has been supported by a grant from Labex OSUG@2020 (Investissements d’avenir—ANR10 LABX56). This work has been carried out within the framework of the NCCR PlanetS supported by the Swiss National Science Foundation. This work has been carried out within the framework of the National

Centre of Competence in Research PlanetS supported by the Swiss National Science Foundation under grants 51NF40\_182901 and 51NF40\_205606. The authors acknowledge the financial support of the SNSF.









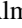
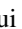









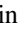

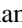

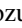






This publication benefits from the support of the French Community of Belgium in the context of the FRIA Doctoral grant awarded to M.T.

The contributions at the Mullard Space Science Laboratory by E.M.B. have been supported by STFC through the consolidated grant ST/W001136/1.

*Facilities:* TESS, HATSouth, MEarth-South, TRAPPIST-South, LCOGT, ExTrA, ESPRESSO, Gaia, Exoplanet Archive.

*Software:* FITSH (Pál 2012), BLS (Kovács et al. 2002), VARTOOLS (Hartman & Bakos 2016), CERES (Brahm et al. 2017a), ZASPE (Brahm et al. 2017b), ODUSSEAS (Antoniadis-Karnavas et al. 2020), AstroImageJ (Collins et al. 2017), TAPIR (Jensen 2013).

## ORCID iDs

Melissa J. Hobson  <https://orcid.org/0000-0002-5945-7975>  
 Andrés Jordán  <https://orcid.org/0000-0002-5389-3944>  
 E. M. Bryant  <https://orcid.org/0000-0001-7904-4441>  
 R. Brahm  <https://orcid.org/0000-0002-9158-7315>  
 D. Bayliss  <https://orcid.org/0000-0001-6023-1335>  
 J. D. Hartman  <https://orcid.org/0000-0001-8732-6166>  
 G. Á. Bakos  <https://orcid.org/0000-0001-7204-6727>  
 Th. Henning  <https://orcid.org/0000-0002-1493-300X>  
 Jose Manuel Almenara  <https://orcid.org/0000-0003-3208-9815>  
 Khalid Barkaoui  <https://orcid.org/0000-0003-1464-9276>  
 Zouhair Benkhaldoun  <https://orcid.org/0000-0001-6285-9847>  
 Xavier Bonfils  <https://orcid.org/0000-0001-9003-8894>  
 François Bouchy  <https://orcid.org/0000-0002-7613-393X>  
 David Charbonneau  <https://orcid.org/0000-0002-9003-484X>  
 Karen A. Collins  <https://orcid.org/0000-0001-6588-9574>  
 Jason D. Eastman  <https://orcid.org/0000-0003-3773-5142>  
 Mourad Ghachoui  <https://orcid.org/0000-0003-3986-0297>  
 Michaël Gillon  <https://orcid.org/0000-0003-1462-7739>  
 Keith Horne  <https://orcid.org/0000-0003-1728-0304>  
 Emmanuel Jehin  <https://orcid.org/0000-0001-8923-488X>  
 Jon M. Jenkins  <https://orcid.org/0000-0002-4715-9460>  
 David W. Latham  <https://orcid.org/0000-0001-9911-7388>  
 Felipe Murgas  <https://orcid.org/0000-0001-9087-1245>  
 Francisco J. Pozuelos  <https://orcid.org/0000-0003-1572-7707>  
 George R. Ricker  <https://orcid.org/0000-0003-2058-6662>  
 Richard P. Schwarz  <https://orcid.org/0000-0001-8227-1020>  
 S. Seager  <https://orcid.org/0000-0002-6892-6948>  
 Andrew Vanderburg  <https://orcid.org/0000-0001-7246-5438>  
 Roland Vanderspek  <https://orcid.org/0000-0001-6763-6562>  
 Joshua N. Winn  <https://orcid.org/0000-0002-4265-047X>

## References

- Almenara, J. M., Bonfils, X., Forveille, T., et al. 2022, *A&A*, 667, L11  
 Anders, F., Khalatyan, A., Queiroz, A. B. A., et al. 2022, *A&A*, 658, A91  
 Antoniadis-Karnavas, A., Sousa, S. G., Delgado-Mena, E., et al. 2020, *A&A*, 636, A9  
 Baraffe, I., & Chabrier, G. 2018, *A&A*, 619, A177

- Bakos, G. Á., Bayliss, D., Bento, J., et al. 2020, *AJ*, 159, 267
- Bakos, G. Á., Csabry, Z., Penev, K., et al. 2013, *PASP*, 125, 154
- Bakos, G. Á., Torres, G., Pál, A., et al. 2010, *ApJ*, 710, 1724
- Bayliss, D., Gillen, E., Eigmüller, P., et al. 2018, *MNRAS*, 475, 4467
- Boss, A. P. 2006, *ApJ*, 643, 501
- Bovy, J., Rix, H.-W., Green, G. M., Schlafly, E. F., & Finkbeiner, D. P. 2016, *ApJ*, 818, 130
- Brahm, R., Jordán, A., & Espinoza, N. 2017a, *PASP*, 129, 034002
- Brahm, R., Jordán, A., Hartman, J., & Bakos, G. 2017b, *MNRAS*, 467, 971
- Brown, T. M., Baliber, N., Bianco, F. B., et al. 2013, *PASP*, 125, 1031
- Burn, R., Schlecker, M., Mordasini, C., et al. 2021, *A&A*, 656, A72
- Caldwell, D. A., Tenenbaum, P., Twicken, J. D., et al. 2020, *RNAAS*, 4, 201
- Canas, C. I., Kanodia, S., Bender, C. F., et al. 2022, *AJ*, 164, 50
- Chabrier, G., & Baraffe, I. 1997, *A&A*, 327, 1039
- Choi, J., Dotter, A., Conroy, C., et al. 2016, *ApJ*, 823, 102
- Claret, A. 2018, *A&A*, 618, A20
- Claret, A., Hauschildt, P. H., & Witte, S. 2012, *A&A*, 546, A14
- Claret, A., Hauschildt, P. H., & Witte, S. 2013, *A&A*, 552, A16
- Collins, K. A., Kielkopf, J. F., Stassun, K. G., & Hessman, F. V. 2017, *AJ*, 153, 77
- Demory, B.-O., & Seager, S. 2011, *ApJS*, 197, 12
- Dotter, A. 2016, *ApJS*, 222, 8
- Dressing, C. D., & Charbonneau, D. 2015, *ApJ*, 807, 45
- Eastman, J. D., Diamond-Lowe, H., & Tayar, J. 2022, arXiv:2209.14301
- Engle, S. G., & Guinan, E. F. 2018, *RNAAS*, 2, 34
- Fausnaugh, M. M., Burke, C. J., Ricker, G. R., & Vanderspek, R. 2020, *RNAAS*, 4, 251
- Freudling, W., Romaniello, M., Bramich, D. M., et al. 2013, *A&A*, 559, A96
- Gagné, J., Mamajek, E. E., Malo, L., et al. 2018, *ApJ*, 856, 23
- Gaia Collaboration, Brown, A. G. A., Vallenari, A., et al. 2018, *A&A*, 616, A1
- Gaia Collaboration, Vallenari, A., Brown, A. G. A., et al. 2022, arXiv:2208.00211
- Gan, T., Lin, Z., Wang, S. X., et al. 2022, *MNRAS*, 511, 83
- García, L. J., Timmermans, M., Pozuelos, F. J., et al. 2022, *MNRAS*, 509, 4817
- Gillon, M., Jehin, E., Magain, P., et al. 2011, in Detection and Dynamics of Transiting Exoplanets, St. Michel l'Observatoire, EPJ Web of Conferences 11, ed. F. Bouchy, R. Díaz, & C. Moutou, 06002
- Guerrero, N. M., Seager, S., Huang, C. X., et al. 2021, *ApJS*, 254, 39
- Hansen, B. M. S., & Barman, T. 2007, *ApJ*, 671, 861
- Hartman, J. D., & Bakos, G. Á. 2016, *A&C*, 17, 1
- Hartman, J. D., Bakos, G. Á., Bayliss, D., et al. 2019, *AJ*, 157, 55
- Hartman, J. D., Bayliss, D., Brahm, R., et al. 2015, *AJ*, 149, 166
- Hippke, M., & Heller, R. 2019, *A&A*, 623, A39
- Hirano, T., Dai, F., Gandolfi, D., et al. 2018, *AJ*, 155, 127
- Hobbs, R., Shorttle, O., & Madhusudhan, N. 2022, *MNRAS*, 516, 1032
- Hsu, D. C., Ford, E. B., & Terrien, R. 2020, *MNRAS*, 498, 2249
- Huang, C. X., Vanderburg, A., Pál, A., et al. 2020a, *RNAAS*, 4, 204
- Huang, C. X., Vanderburg, A., Pál, A., et al. 2020b, *RNAAS*, 4, 206
- Hut, P. 1981, *A&A*, 99, 126
- Irwin, J. M., Berta-Thompson, Z. K., Charbonneau, D., et al. 2015, in Cambridge Workshop on Cool Stars, Stellar Systems, and the Sun. Proc. of the conf. held at Lowell Observatory 18, ed. G. van Belle & H. C. Harris, 767
- Jao, W.-C., Henry, T. J., Gies, D. R., & Hambly, N. C. 2018, *ApJL*, 861, L11
- Jehin, E., Gillon, M., Queloz, D., et al. 2011, *Msngr*, 145, 2
- Jenkins, J. M., Twicken, J. D., McCauliff, S., et al. 2016, *Proc. SPIE*, 9913, 99133E
- Jensen, E. 2013, Tapir: A web interface for transit/eclipse observability, Astrophysics Source Code Library, record ascl:1306.007
- Johnson, J. A., & Apps, K. 2009, *ApJ*, 699, 933
- Johnson, J. A., Gazak, J. Z., Apps, K., et al. 2012, *AJ*, 143, 111
- Jordán, A., Hartman, J. D., Bayliss, D., et al. 2022, *AJ*, 163, 125
- Kanodia, S., Mahadevan, S., Libby-Roberts, J., et al. 2023, *AJ*, 165, 120
- Kempton, E. M.-R., Bean, J. L., Louie, D. R., et al. 2018, *PASP*, 130, 114401
- Kovács, G., Bakos, G., & Noyes, R. W. 2005, *MNRAS*, 356, 557
- Kovács, G., Zucker, S., & Mazeh, T. 2002, *A&A*, 391, 369
- Kunimoto, M., Daylan, T., Guerrero, N., et al. 2022, *ApJS*, 259, 33
- Laughlin, G., Bodenheimer, P., & Adams, F. C. 2004, *ApJL*, 612, L73
- Lillo-Box, J., Figueira, P., Leleu, A., et al. 2020, *A&A*, 642, A121
- Mandel, K., & Agol, E. 2002, *ApJL*, 580, L171
- Mann, A. W., Dupuy, T., Kraus, A. L., et al. 2019, *ApJ*, 871, 63
- McCully, C., Volgenau, N. H., Harbeck, D.-R., et al. 2018, *Proc. SPIE*, 10707, 107070K
- Miller, N., & Fortney, J. J. 2011, *ApJL*, 736, L29
- Modigliani, A., Freudling, W., Anderson, R. I., et al. 2020, in ASP Conf. Ser. 527, Astronomical Data Analysis Software and Systems XXIX, ed. R. Pizzo et al. (San Francisco, CA: ASP), 667
- Mollière, P., Molyarova, T., Bitsch, B., et al. 2022, *ApJ*, 934, 74
- Morales, J. C., Mustill, A. J., Ribas, I., et al. 2019, *Sci*, 365, 1441
- Mordasini, C., Alibert, Y., Georgy, C., et al. 2012, *A&A*, 547, A112
- Mulders, G. D. 2018, in Planet Populations as a Function of Stellar Properties, ed. H. J. Deeg & J. A. Belmonte (Berlin: Springer), 153
- Nutzman, P., & Charbonneau, D. 2008, *PASP*, 120, 317
- Pál, A. 2012, *MNRAS*, 421, 1825
- Pascucci, I., Testi, L., Herczeg, G. J., et al. 2016, *ApJ*, 831, 125
- Paxton, B., Bildsten, L., Dotter, A., et al. 2011, *ApJS*, 192, 3
- Paxton, B., Cantiello, M., Arras, P., et al. 2013, *ApJS*, 208, 4
- Paxton, B., Marchant, P., Schwab, J., et al. 2015, *ApJS*, 220, 15
- Pecaut, M. J., & Mamajek, E. E. 2013, *ApJS*, 208, 9
- Penev, K., Bakos, G. Á., Bayliss, D., et al. 2013, *AJ*, 145, 5
- Pepe, F., Cristiani, S., Rebolo, R., et al. 2021, *A&A*, 645, A96
- Rabus, M., Lachaume, R., Jordán, A., et al. 2019, *MNRAS*, 484, 2674
- Ricker, G. R., Winn, J. N., Vanderspek, R., et al. 2015, *JATIS*, 1, 014003
- Rojas-Ayala, B., Covey, K. R., Muirhead, P. S., & Lloyd, J. P. 2010, *ApJL*, 720, L113
- Roulston, B. R., Green, P. J., & Kesseli, A. Y. 2020, *ApJS*, 249, 34
- Sarkis, P., Mordasini, C., Henning, T., Marleau, G. D., & Mollière, P. 2021, *A&A*, 645, A79
- Schlecker, M., Burn, R., Sabotta, S., et al. 2022, *A&A*, 664, A180
- Shaklan, S., Bonfils, X., Almenara, J. M., et al. 2015, *Proc. SPIE*, 9605, 96051L
- Silverstein, M. L., Schlieder, J. E., Barclay, T., et al. 2022, *AJ*, 163, 151
- Skrutskie, M. F., Cutri, R. M., Stiening, R., et al. 2006, *AJ*, 131, 1163
- Smith, J. C., Stumpe, M. C., Van Cleve, J. E., et al. 2012, *PASP*, 124, 1000
- Sosnowska, D., Lovis, C., Figueira, P., et al. 2015, in ASP Conf. Ser. 495, Astronomical Data Analysis Software and Systems XXIV (ADASS XXIV), ed. A. R. Taylor & E. Rosolowsky (San Francisco, CA: ASP), 285
- Southworth, J. 2011, *MNRAS*, 417, 2166
- Stumpe, M. C., Smith, J. C., Catanzarite, J. H., et al. 2014, *PASP*, 126, 100
- Stumpe, M. C., Smith, J. C., Van Cleve, J. E., et al. 2012, *PASP*, 124, 985
- Tayar, J., Claytor, Z. R., Huber, D., & van Saders, J. 2022, *ApJ*, 927, 31
- Thorgren, D. P., Fortney, J. J., Murray-Clay, R. A., & Lopez, E. D. 2016, *ApJ*, 831, 64
- Triaud, A. H. M. J., Anderson, D. R., Collier Cameron, A., et al. 2013, *A&A*, 551, A80
- Twicken, J. D., Catanzarite, J. H., Clarke, B. D., et al. 2018, *PASP*, 130, 064502
- van Saders, J. L., & Pinsonneault, M. H. 2012, *ApJ*, 751, 98